Static and dynamic magnetic properties of an $[Fe_{13}]$ cluster

Joris van Slageren,[1,*] Patrick Rosa,[1,†] Andrea Caneschi,[1] Roberta Sessoli,[1,‡] Hélène Casellas,[1,§] Yuri V. Rakitin,[1,2] Luciano Cianchi,[3] Franco Del Giallo,[3] Gabriele Spina,[4] Avi Bino,[5] Anne-Laure Barra,[6] Tatiana Guidi,[7] Stefano Carretta,[8] and Roberto Caciuffo[7,‖]

[1]*INSTM, UdR Firenze, and Laboratorio di Magnetismo Molecolare, Università degli Studi di Firenze, Via della Lastruccia, 3, I-50019, Sesto Fiorentino (FI), Italy*

[2]*Institute of Chemistry, Fersman Str. 14, 184200 Apatity, Murmansk reg., Russia*

[3]*ISC, CNR, Via Madonna del piano, 50019 Sesto Fiorentino (FI), Italy*

[4]*INFM-Firenze, Dipartimento di Fisica, Università di Firenze, Via G. Sansone 1, I-50019 Sesto Fiorentino (FI), Italy*

[5]*Department of Inorganic and Analytical Chemistry, The Hebrew University of Jerusalem, 91904 Jerusalem, Israel*

[6]*Laboratoire des Champs Magnétiques Intenses, CNRS UPR5021, BP 166 F-38402 Grenoble Cedex 9, France*

[7]*Dipartimento di Fisica ed Ingegneria dei Materiali e del Territorio, Università Politecnica delle Marche, Via Brecce Bianche, I-60131 Ancona, Italy*

[8]*INFM and Dipartimento di Fisica, Università di Parma, Parco Area delle Scienze 7A, I-43100 Parma, Italy*

(Received 19 September 2005; published 24 January 2006)

The static and dynamic magnetic properties of an $[Fe_{13}]$ cluster were investigated using several experimental techniques. The cluster crystallizes in a cubic space group, but careful investigation of the crystallographic data revealed that the symmetry is distorted locally. dc magnetic susceptibility measurements showed the presence of competing antiferromagnetic isotropic exchange interactions leading to a high-spin ground state and many low-lying excited spin states, which was confirmed by inelastic neutron scattering measurements. From high-field electron paramagnetic resonance measurements a small zero-field splitting of the spin ground state was inferred, which supports the local symmetry distortion found in the crystallographic studies. The spin dynamics slows down at sub-kelvin temperatures, where ac susceptibility measurements indicated that part of the sample shows superparamagnetic-like behavior and the other part relaxes through magnetization tunneling. The Mössbauer data confirmed the slowing down of the spin dynamics, indicating that this occurs mainly in the peripheral spins.

DOI: 10.1103/PhysRevB.73.014422 PACS number(s): 75.50.Xx, 75.40.Gb, 76.30.−v, 76.80.+y

INTRODUCTION

In certain cases the lattice geometry gives rise to the interesting phenomenon of spin frustration, of which one famous example is the Kagome lattice.[1] Central to such lattices is the presence of triangular exchange interaction geometries. The studied systems are generally extended two-dimensional lattices. If the lattice were curved in both dimensions, as it would be projected on a sphere, a highly symmetric zero-dimensional object would result, which can be expected to show interesting properties due to that high symmetry and also due to the finite size of the lattice. An example of a highly symmetric, frustrated molecular system is the polyoxomolybdate cluster $[Fe_{30}Mo_{72}]$ which contains 30 iron(III) ions $\left(s=\frac{5}{2}\right)$ in an icosadodecahedral arrangement.[2] This system suffers from the drawback that the effective isotropic superexchange interaction is rather weak, of the order of $J=1.5\ cm^{-1}$, due to the long and inefficient superexchange pathways. Recently, an iron(III) system was published,[3] which can be expected to show stronger exchange interaction due to the presence of monoatomic bridges between the paramagnetic ions which can efficiently transmit superexchange interactions, and in addition to show a high degree of spin frustration. This tridecanuclear Fe^{III} compound, $(C_5H_6N^+)_5[Fe_{13}F_{24}(OCH_3)_{12}O_4]\cdot CH_3OH\cdot 4H_2O$ $(\equiv[Fe_{13}])$ crystallizes in the cubic space group F-43*m*. Due to its high symmetry there are only two independent Fe^{III} ions in the molecule, viz., one in the center and one other, which is reproduced 12 times due to the symmetry elements of the space group. Although only four pyridinium cations were found in the x-ray diffractions studies, the presence of a fifth one was assumed, since an overall charge of −4 of the cluster anion would suggest an unrealistic +4 oxidation state of the central iron ion: the presence of five pyridinium cations, corroborated by elemental analysis and volumetric titration, excluded the presence of Fe(IV) ions. Preliminary magnetic measurements indicated a complicated dependence of the magnetic susceptibility on temperature and suggested a high-spin ground state. Mössbauer spectroscopic data supported the +3 oxidation state of all iron ions, but no magnetic structure was observed.[3]

The other point of interest in such exchange-coupled clusters is the fact that many of them show the phenomenon of slow relaxation of the magnetization due to the zero-field splitting (ZFS) of the spin ground state. This zero-field splitting lifts the degeneracy of the spin ground state, effectively leading to an energy barrier towards the relaxation of the magnetization. In addition, transverse terms in the spin Hamiltonian can lead to tunneling of the magnetic moment under the barrier. Such terms are not allowed by symmetry in second order if the symmetry is tetragonal or higher. In cubic symmetry, in fact, no ZFS is expected at all below fourth order. Recently, it has been shown that local lowering of the symmetry due to disorder in the system can lead to the presence of lower order transverse terms. It is clear that disorder

can play a major role in highly symmetric systems.

Here we report the study of the static and dynamic magnetic properties of the mentioned cubic symmetry $[Fe_{13}]$ cluster, using a number of experimental techniques, which shows that especially the spin dynamics are to a large extent governed by disorder.

EXPERIMENTAL SECTION

$(C_5H_6N^+)_5[Fe_{13}F_{24}(OCH_3)_{12}O_4]\cdot CH_3OH\cdot 4H_2O$ ($[Fe_{13}]$) was synthesized as published recently.[3] The deuterated derivative for inelastic neutron scattering (INS) experiments was prepared and stocked under inert atmosphere by using fully deuterated methanol.

dc and ac magnetic susceptibilities and the magnetization were measured on powder samples, using a Cryogenics S600 superconducting quantum interference device (SQUID) magnetometer and an Oxford VSM with a 12 T magnet. The data were corrected for the diamagnetic contribution using Pascal's constants. Low-temperature ac magnetic susceptibility data were measured in a custom-designed susceptometer based on an Oxford ^{3}He Heliox cryostat, a SR830 lock-in serving also as the ac current source, an Oxford ITC 503 temperature controller, and a homemade probe built by Professor M. A. Novak, Universidade Federal do Rio de Janeiro, Brazil. The temperature was measured with a calibrated RuO_2 probe below 4 K; magnetic calibration was done with a spherical ferrimagnetic sample previously calibrated with SQUID dc measurements.

Inelastic Neutron Scattering measurements were performed at the Institute Laue-Langevin (ILL) in Grenoble (France), with the direct-geometry time-of-flight spectrometer IN5. About 1.7 g of deuterated polycrystalline sample were placed in a hollow aluminum cylinder (0.7 mm wall thickness, 20 mm inner diameter), and inserted into a standard ILL ^{4}He cryostat allowing a base temperature of 2 K. The spectrometer was operated in high and medium energy resolution configurations, with incident wavelengths $\lambda = 11$ Å and $\lambda = 6$ Å, corresponding to energy resolution at the elastic peak of 12 and 60 μeV, respectively. Solid angle and detector efficiency calibrations have been performed using the spectrum of a vanadium standard.

The low-energy-transfer region was explored with the IN16 spectrometer at the ILL. In this instrument high energy resolution is achieved by deflecting the neutrons at the monochromator and at the analyzer with a Bragg angle of 90°. The energy of the incident beam is varied by Doppler motion of the monochromator. By using a spherically shaped Si(111) monochromator and deformed Si(111) single crystals as analyzers, an energy resolution of 0.9 μeV is obtained over an energy transfer range from -15 to 15 μeV. For this experiment, a cylindrical aluminum holder containing 1.2 g of material was used inside a dilution refrigerator allowing the sample to be cooled to a minimum temperature of 50 mK.

HF-EPR spectra of $[Fe_{13}]$ pellets were recorded on a home made spectrometer,[4,5] operating in the single-pass transmission mode. The main magnetic field is supplied by a superconducting magnet (Cryogenics Consultants) with a maximum field of 12 T. Gunn-diodes and their multipliers (Radiometer Physics) were used as frequency sources, with a basic frequency of 95 or 115 GHz.

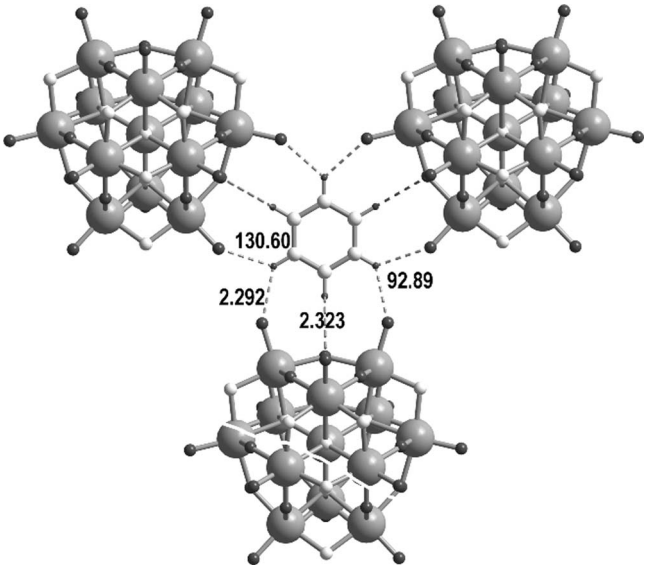

FIG. 1. View along the [111] axis, showing one pyridinium cation and the three surrounding clusters, emphasizing the crystal packing. The big spheres in the clusters are Fe^{III} ions, the small, light spheres are oxygen atoms, and the small, dark spheres are fluoride ions. The methanolate methyl groups have been omitted for clarity.

For the Mössbauer experiments powdered $[Fe_{13}]$ was mixed with eicosane (Aldrich) and compressed inside a disk-shaped holder. The effective thickness of the iron was 4.1 mg cm^{-2}. The spectra were recorded by using a conventional sinusoidal acceleration spectrometer that operated in a multichannel scaling mode. The γ-ray source, which consisted of 25 mCi of ^{57}Co in a rhodium metal matrix, was maintained at room temperature. A natural abundance iron foil was used to calibrate the spectrometer. The measurements were performed in a standard exchange helium cryostat (Oxford, Inc.), using a control program under LabView.

RESULTS AND DISCUSSION

X-ray diffraction

The structure of $[Fe_{13}]$ as determined previously, is shown in Fig. 1. The cluster itself is highly symmetric, with the central iron ion lying on a T_d symmetry site, and only one independent further iron ion. Closer inspection of the crystal structure revealed that the cluster is surrounded by 12 pyridinium cations, bound by hydrogen bonds between the pyridinium ions and the cluster (Fig. 1). The aromatic hydrogen atoms are relatively weak hydrogen bond donors, while the N^+-H groups are expected to be much stronger, of the order of 4 kcal mol^{-1}.[6] Both terminal Fe-F and bridging Fe-F-Fe fluoride ions can act as acceptors. Since the hydrogen bonds formed with N^+-H donors have been found to be much more directional, with angles close to linear,[7] it can be assumed that the N^+-H groups of the pyridinium ions will preferentially bind to the bridging Fe-F-Fe groups.

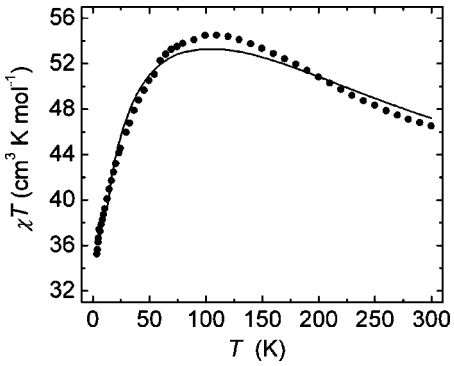

FIG. 2. Observed (●) and calculated (—) χT values. The molar magnetic susceptibility data were recorded at an applied field of $H=0.1$ T. The fit was obtained with $J_1=43$ cm^{-1} and $J_2=30$ cm^{-1}.

Two factors are expected to lead to local distortions of the lattice, leading to local symmetry lowering of the cluster molecules. First of all, of the five pyridinium cations that are required for charge neutrality only four could be found in the single crystal x-ray analysis, the fifth being disordered to such an extent that is does not show up in the electron density difference maps. That means that the tetrahedral lattice formed by the hydrogen bonded network of pyridinium ions and $[Fe_{13}]^{5-}$ clusters contains inclusions of the fifth pyridinium ion at nonspecific sites, leading to local distortion of the lattice. The same argument holds for the co-crystallized water and methanol molecules which are both good hydrogen donors. Secondly, the strong hydrogen bond formed between the N^+-H moiety and the Fe-F-Fe bridge can induce a local distortion of that bridge, leading to a local lowering of the cluster symmetry, because each N^+-H group can bind to only one cluster.

dc magnetic susceptibility

Preliminary susceptibility measurements suggested the presence of strong antiferromagnetic intracluster exchange interactions. In fact, the observed room temperature χT product of 46.5 cm^3 K mol^{-1} (Fig. 2) is much lower than that expected for 13 noninteracting iron(III) ions $[\chi T=N\times 0.125\times g^2\times S(S+1)=56.9$ cm^3 K mol$^{-1}]$. The rise of χT on lowering the temperature to a maximum value of 54.5 cm^3 K mol^{-1} at 109.5 K suggests ferrimagnetic interactions, which is supported by the observation that the susceptibility does not tend to zero at low temperatures. A Curie-Weiss plot of the low-temperature part ($T<6$ K) yields a Curie constant of $C=39.8\pm0.3$ cm^3 K mol^{-1}, close to that expected for $S=\frac{17}{2}$ and $g=2.0$, assuming that only the ground spin multiplet is populated. The Weiss temperature is $\theta=-0.41\pm0.04$ K, which could indicate small intermolecular antiferromagnetic interactions. The value of the magnetic moment of $\mu=20\mu_B$ at $H=12$ T (not shown) also indicates a high-spin ground state, while the fact that the magnetization does not saturate even at these fields suggests the presence of low-lying excited spin multiplets with larger spin multiplicity.

In spite of the high symmetry, the spin topology is quite complicated and quite frustrated, due to the presence of eight

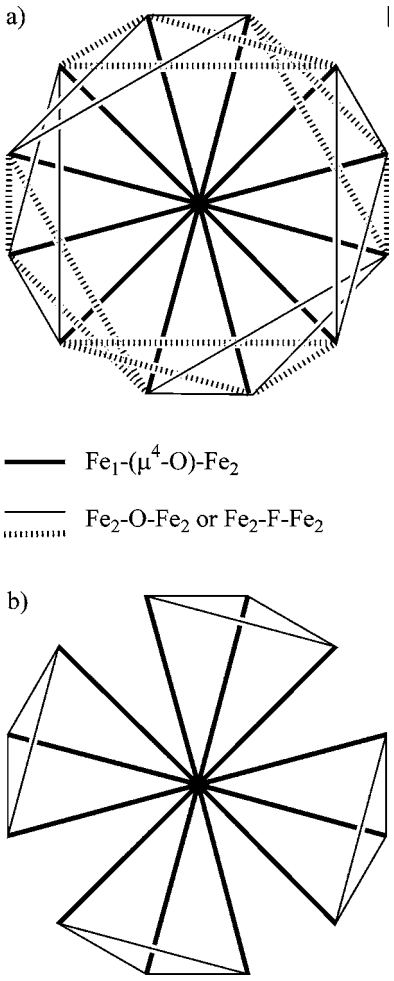

FIG. 3. (a) Spin topology of $[Fe_{13}]$. (b) Spin topology after neglecting one of the intratriangle interactions.

triangular interactions [Fig. 3(a)]. In $[Fe_{13}]$ there are three types of exchange interactions, which are all expected to have significant magnitude. The central iron ion (Fe1) interacts with all other iron ions (Fe2) through μ^4-oxo bridges (O1). These bridges are asymmetric since the Fe1-O1 distance is short [1.888(6) Å], while Fe2-O1 is 2.093(3) Å. In oxo-bridged iron(III) dimers it has been found that the exchange interaction decreases with increasing Fe-O distance, while the Fe-O-Fe angle dependence is less clear.[8] In polynuclear complexes,[9] and alkoxo-bridged dinuclear complexes[10] a definite angle dependence was observed with the exchange interaction becoming more antiferromagnetic with increasing Fe-O-Fe angles. The short Fe1-O1 distance in $[Fe_{13}]$, combined with $\angle$Fe1-O1-Fe2=120.77(13)°, suggests that there should be a relatively strong antiferromagnetic interaction between Fe1 and Fe2. The peripheral iron ions (Fe2) interact in two different ways. The first is through a combination of said μ^4-oxo bridge, with $\angle$Fe2-O1-Fe2 =96.16(18)°, combined with a methoxide bridge (O2), with $\angle$Fe2-O2-Fe2=104.60(18)°, and a Fe2-O2 distance of 1.968 Å. The second is through a fluoride bridge, with $\angle$Fe2-F-Fe2=146.97(16)°. The exchange path through O1 is expected to give rise to a weakly antiferromagnetic or even ferromagnetic exchange interaction in view of the small

∠Fe2-O1-Fe2 of 96.16(18)°.[9] Both other exchange paths between the different Fe2 atoms are expected to give rise to similar exchange interaction strengths, since the Fe2-O2-Fe2 angle of 104.60(18)° and the Fe2-O2 distance of 1.968 Å favor an antiferromagnetic exchange interaction between the Fe2 atoms, as do the ∠Fe2-F-Fe2 angle of 146.97(16)° and the Fe2-F distance of 1.979(1) Å. For example, for the Fe-F-Fe interaction in the rhombohedral phase of FeF_3, with an Fe-F distance of 1.92 Å and ∠Fe-F-Fe=152°, a superexchange interaction of $J=17-20$ cm^{-1} was estimated.[11]

It is immediately clear that a stronger Fe1…Fe2 exchange interaction will lead to a high-spin ground state (up to $S=\frac{55}{2}$), while a stronger Fe2…Fe2 exchange interaction will give rise to a low-spin system. The susceptibility data point to the former case. However, despite the high symmetry of the system, its size precludes a fit of the susceptibility curve to an isotropic exchange interaction Hamiltonian using numeric diagonalization methods. Even when making full use of the symmetry of the system using irreducible tensor operator methods, the dimension of the largest matrix is still ca. 80,000,000. The only possibility to obtain insight into the strengths of the exchange interactions is by neglecting one of the two Fe2…Fe2 exchange interactions. While such a procedure is not expected to lead to an accurate description of the spin state energies, it will give information on the relative strengths of the Fe1…Fe2 and Fe2…Fe2 exchange interactions as well as the approximate value of the spin ground state.

After neglecting one of the Fe2…Fe2 interactions the spin topology simplifies enormously [Fig. 3(b)]. In fact, since the system can be divided into two subsystems (one consisting of four triangles and one of the central spin) where the interactions between all the members of one subsystem and all the members of the other subsystem are equal, the problem has an analytical solution.[12] This approach, called the Kambe approach after its inventor,[13] has been used in several instances for clusters of up to nine spins.[14,15] The spin Hamiltonian is

$$H = J_2(S_1S_2 + S_2S_3 + S_3S_1 + S_4S_5 + S_5S_6 + S_6S_4 + S_7S_8 + S_8S_9 + S_9S_7 + S_{10}S_{11} + S_{11}S_{12} + S_{12}S_{10}) + J_1\left(S_{13}\sum_{i=1}^{12} S_i\right) \quad (1)$$

where S_1-S_{12} correspond to the symmetry generated crystallographic Fe2 type ions, and S_{13} corresponds to the Fe1 ion. J_1 and J_2 describe the Fe1…Fe2 exchange interaction and the intratriangle Fe2…Fe2 one, respectively. Following the Kambe approach, the system under study is divided into two subsystems, one being the central iron atom (S_{13}) and the other being the outer iron atoms (S_{1-12}). All spins in the first subsystem are connected to those in the second subsystem by equivalent coupling constants J_1. The S_{1-12} system is then divided into the systems S_{1-6} and S_{7-12}, which are again connected by equivalent (in this case zero) interactions. Finally the two subsystems S_{1-6} and S_{7-12} are divided into the triangles S_{1-3}, S_{4-6}, S_{7-9}, and S_{10-12}. For these latter triangular systems the analytical solution of the SH is known. Eventually the exact solution of the SH of the system under study is obtained:

$$E = J_1/2[S_{1-13}(S_{1-13}+1) - S_{1-12}(S_{1-12}+1)] + J_2/2[S_{1-3}(S_{1-3}+1) + S_{4-6}(S_{4-6}+1) + S_{7-9}(S_{7-9}+1) + S_{10-12}(S_{10-12}+1)]. \quad (2)$$

The total spin function is

$$|S_1S_2S_{1-2}S_3S_{1-3}S_4S_5S_{4-5}S_6S_{4-6}S_7S_8S_{7-8}S_9S_{7-9}S_{10}S_{11}S_{10-11}S_{12}S_{10-12}S_{1-6}S_{7-12}S_{1-12}S_{13}S_T\rangle.$$

From this formula, it is clear that the energy of a spin state only depends on the spin states of the four triangles, the way they are coupled and the way they are coupled to the central Fe atom. Figure 4 shows the energies of the ~250 lowest spin states as a function of the ratio between the intratriangle exchange interaction and the central-peripheral exchange interaction, with the consecutive spin ground states as bold lines. In this model, the degeneracies of the low-lying excited states is very large, which would be partially removed by the inclusion of the second type of Fe2…Fe2 interaction. The possible spin states of each triangle are $S=\frac{15}{2}, \frac{13}{2}, \frac{11}{2}, \ldots, \frac{1}{2}$, and the total spin S_T is expected to assume any value between $\frac{1}{2}$ and $\frac{65}{2}$. However, given the high symmetry of the system, the spin ground states as a function of J_2/J_1 assume only those values arising from an identical contribution of all four triangles. As the resulting intermediate spin S_{1-12} is coupled antiferromagnetically to the central ion spin, on increasing the antiferromagnetic J_2 interaction the

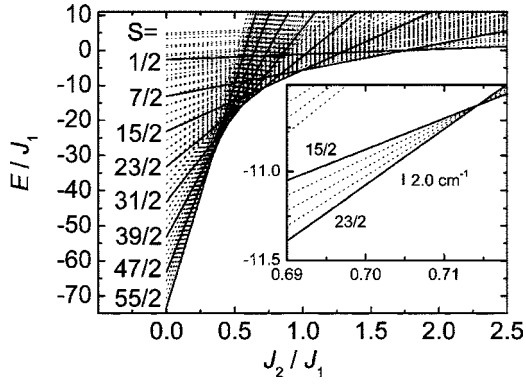

FIG. 4. Plot of the energies of the various spin levels as a function of the ratio of the exchange interaction constants, J_2/J_1. The inset shows the low-lying spin states in the $J_2/J_1=0.70$ region which is the J_2/J_1 ratio that results from the fit (see text). The bar indicates the energy scale for the fitted value of $J_1=43$ cm^{-1}.

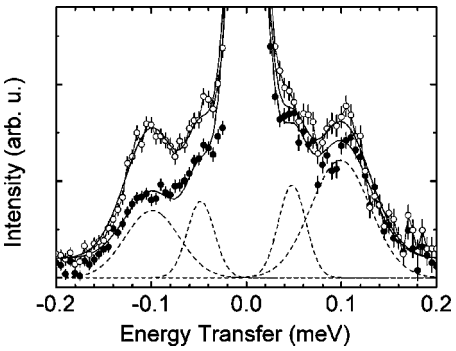

FIG. 5. INS spectra recorded on IN5 using incident neutrons with $\lambda=11$ Å (energy resolution 12 μeV). Data have been collected at $T=2$ K (closed circles) and $T=10$ K (open circles). Solid lines represent the superposition of the elastic peak and four Gaussian line shapes centered at ±0.05 and ±0.10 meV. Individual components are shown by broken lines.

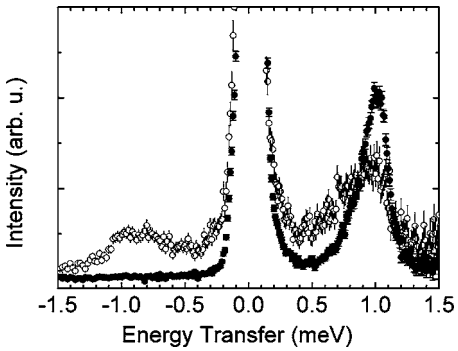

FIG. 6. INS spectra recorded on IN5 using incident neutrons with $\lambda=6$ Å (energy resolution 60 μeV). Data have been collected at $T=2$ K (closed circles) and $T=15$ K (open circles). The intensity results from the sum over the whole detector bank, covering an angular range from 14.5°–132.5°.

consecutive spin ground states of the cluster are expected to be $S_T=\frac{55}{2},\frac{47}{2},\frac{43}{2},\ldots,\frac{1}{2}$.

The magnetic susceptibility can be calculated from the summation over all spin states i of total spin S_T^i and energy E_i:

$$\chi^T=\frac{Ng^2\mu_B^2}{3k}\frac{\sum_i S_T^i(S_T^i+1)(2S_T^i+1)\exp(-E_i/kT)}{\sum_i(2S_T^i+1)\exp(-E_i/kT)}. \quad (3)$$

Using a home written program, χT was fitted to the experimental data (Fig. 2). The resulting J_1 and J_2 values are about 43 and 30 cm^{-1}, respectively, although the J_2/J_1 ratio (0.70) is probably more reliable than the actual values. This J_2/J_1 ratio would then suggest within our model that the spin ground state of the Fe_{13} cluster is either $S_T=\frac{23}{2}$ or $S_T=\frac{15}{2}$. Those values are an indication that the Fe2…Fe2 and Fe1…Fe2 interactions are of comparable magnitude, which leads to a large spin ground state. Exactly at $J_2/J_1=0.70$, the spin ground state is $S_T=\frac{23}{2}$, while the excited states have progressively lower spin values of $S_T=\frac{21}{2}$, $\frac{19}{2}$, $\frac{17}{2}$, and $\frac{15}{2}$ with the separation between the states being $\Delta E=0.05J_1$, corresponding to $\Delta E=2.15$ cm^{-1} for $J_1=43$ cm^{-1} (inset of Fig. 4).

Inelastic neutron scattering

INS is the zero-field technique of choice to obtain information on the total spin energy levels in exchange-coupled clusters because of the $\Delta S=0,\pm1$ selection rule for INS transitions (in addition to the $\Delta M_S=0,\pm1$ selection rule).[16] In this study we focus especially on the low-energy region to verify the presence of low-lying excited spin states, in a series of different measurements. First of all, a very-high resolution experiment on the IN16 backscattering spectrometer at temperatures of $T=55$ mK and $T=500$ mK showed no inelastic transitions in the accessible energy transfer range of up to 15 μeV. Secondly, the magnetic response up to 1.5 meV was explored with lower resolution using the IN5 chopper spectrometer. Figure 5 shows the INS intensity distribution recorded with the sample kept at $T=2$ K and $T=10$ K, and an incident wavelength of $\lambda=11$ Å. Counts in individual detectors at different scattering angles were summed before the time-of-flight to energy conversion. Background, detector efficiency, and absorption corrections have been applied following standard procedures. Two peaks are clearly resolved both on the energy-gain and the energy-loss side of the spectrum. They can be fitted to Gaussian line shapes centered at ±50(5) μeV and ±99(6) μeV (0.40 and 0.79 cm^{-1}, respectively) and having a full width at half maximum (FWHM) about three and six times the instrumental resolution (12 μeV), respectively. These wide peaks can arise from several types of transitions. First, they can be due to excitations between ground spin manifolds (formed by different equivalent topological configurations) and close-lying spin multiplets described by a density of states peaked at 50 and 99 μeV. Second, transitions across a small gap created by static geometric distortions were recently shown to be the cause of the observation of a 35 μeV gap in $[V_{15}]$ in INS measurements, and similar phenomena could occur in the present system.[17] Finally, attribution to intra multiplet transitions between different M_S states is a possibility (see HFEPR results below).

Two further excitation bands are observed at higher-energy transfer, as shown in Fig. 6, where the results of measurements performed with IN5 and an incident wavelength of $\lambda=6$ Å are reported. At $T=2$ K, a broad peak is observed in the neutron energy-loss side at about 1.0 meV (8.0 cm^{-1}). On warming, the intensity of this excitation band decreases, while a second band increases in intensity at lower energy. At $T=15$ K, the INS response can be fitted to the sum of a Gaussian centered at 0.7 meV (5.6 cm^{-1}), with FWHM of 0.5 meV (almost an order of magnitude larger than the resolution), and one centered at 1.0 meV, having a FWHM of 0.25 meV (four times the resolution). These results suggest the presence of many spin energy levels closely spaced around a mean value of 1 and 1.7 meV. These bands undoubtedly belong to $\Delta S=0,\pm1$ transitions from the ground state (1.0 meV) and between excited states (0.7 meV).

High-field EPR (HFEPR)

Figure 7 shows the HFEPR spectra recorded on a pressed powder sample at 285 GHz at various temperatures. The in-

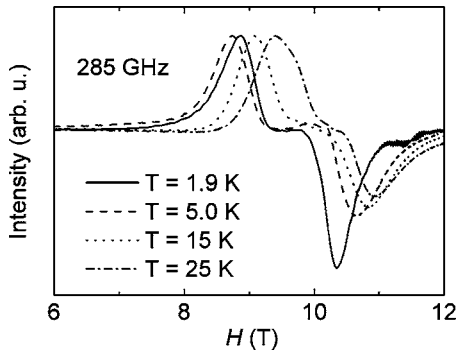

FIG. 7. High-frequency EPR spectra recorded on a pressed powder sample of $[Fe_{13}]$ at $\nu=285$ GHz at various temperatures as indicated in the figure.

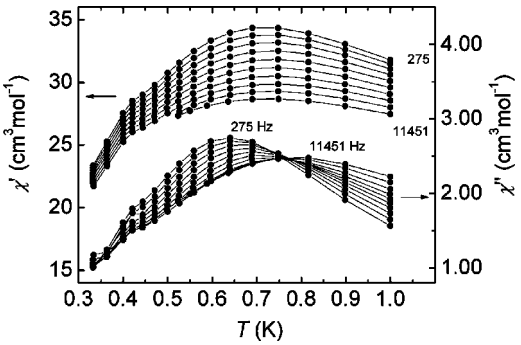

FIG. 8. The real (χ', top) and imaginary (χ'', bottom) parts of the ac susceptibility recorded in zero applied field at various driving frequencies ranging between 275 and 11451 Hz as indicated in the figure.

tensities have been normalized to facilitate comparison. Further HFEPR spectra were recorded at 190 GHz. At high temperatures, a broad resonance line is observed which is centered around $g=2.01\pm0.01$. On lowering the temperature, first the peak-to-peak separation increases and the line shifts to lower field (higher g value). At the lowest temperature of $T=1.9$ K, the peak-to-peak separation again decreases somewhat, and $g=2.14\pm0.01$, but no well-resolved structure can be observed. The resonance lines can be attributed to the sum of excitations within several total spin multiplets. At high temperatures many of these multiplets are thermally populated, while lowering of the temperature leads to preferential population of the lowest spin multiplets, which can explain the shift in g value. The plateau between the two peaks as well as the temperature dependence of the peak-to-peak separation suggest the presence of zero-field splitting. For strict cubic symmetry, ZFS can only be present from fourth order, where the spin Hamiltonian will include a term like $\Sigma\hat{S}_{\alpha}^{4}$ ($\alpha=x,y,z$), which leads to the presence of three perpendicular unique axes. However, small deviations from perfect cubic symmetry are expected to lead to a sizeable second order ZFS. For instance, it was shown that small deviations from tetragonal symmetry can lead to a significant second order transverse anisotropy.[18,19] If such small distortions are indeed present, then from the HFEPR spectra an estimate of the ZFS D parameter can be obtained: Assuming that at the lowest temperature only the lowest spin multiplet is populated, in the strong field limit, the resonance field difference between lowest and highest field transition cannot be more than $(2S-1)D/g\mu_B$ for half-integer spins. The peak-to-peak separation at $T=1.9$ K and $\nu=285$ GHz is $\Delta H\approx1.5$ T. For $S=\frac{15}{2}$ (the low end of the possible S values for the total spin of the ground state) this leads to a maximum axial ZFS of $|D|\approx0.1$ cm^{-1}.

ac susceptibility

In agreement with the small ZFS estimate obtained from HFEPR, no χ'' (out-of-phase or imaginary component of the ac susceptibility) signal is observed in ac susceptibility measurements down to $T=2.0$ K, showing that at these temperatures the magnetization dynamics are relatively fast. At temperatures below 1 K, however, a small but reproducible χ'' signal is observed, which goes through a maximum as a function of temperature (Fig. 8). The temperature corresponding to the maximum of this χ'' signal is frequency dependent ranging from $T_{max}=560$ mK for $\nu=15$ Hz to $T_{max}=800$ mK for $\nu=17\,329$ Hz. The real part (χ') also shows a maximum as a function of temperature, which, in contrast, is virtually frequency independent over the frequency range employed ($T_{max}=700$ mK). The magnitude of the χ' signal does depend on frequency, increasing by almost 20% going from the highest to the lowest frequency. Finally, χ'' is an order of magnitude smaller than χ'. At lower temperatures ($T\approx420$ mK) there seems to be an additional feature in both χ' and χ'', which will not be discussed here.

The appearance of a nonzero χ'' can be due to several physical phenomena. We can exclude a long range order magnetic phase transition, because this gives a frequency-independent χ'' signal at the critical temperature. On the contrary, superparamagnetic or single-molecule-magnet behavior is characterized by an out-of-phase component χ'', and a decrease in χ' on lowering the temperature, with the maximum in χ'' corresponding to the inflection point in χ'. Furthermore both χ' and χ'' are strongly frequency dependent, as observed for $[Fe_{13}]$. However, if the relaxation process is described by one characteristic relaxation time, the values of χ'' and χ' are the same at the temperature corresponding to the maximum in χ'',[17] in contrast with our observation of a significantly smaller χ''. The relaxation time as a function of temperature in single molecule magnets can be described well by the Arrhenius law. An intermediate case is constituted by spin glasses where the broad distribution in relaxation times leads to a much smaller χ'' signal compared to χ' (typically one to two orders of magnitude).[17] The χ' signal however shows a maximum ("cusp") as a function of temperature, which shifts to lower temperature with decreasing frequency. The frequency shift for spin glasses is defined as $\Delta T_f/T_f\Delta(\log_{10}\omega)$, where T_f is the temperature at the maximum in χ'', and is typically of the order of a few percent per decade in frequency, reaching 6% for insulating spin-glass-like materials. Around the temperature of the maximum in χ', χ'' would rise quickly, and the temperature at which the slope in χ'' is largest would correspond to the maximum in χ'. This means that also in spin glasses the frequency shifts

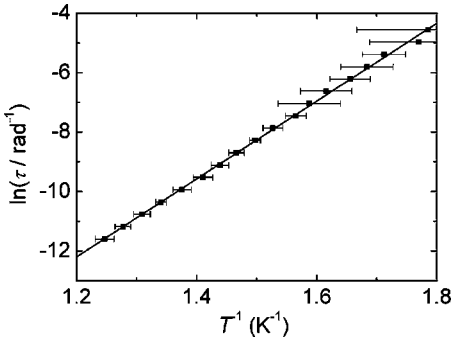

FIG. 9. Measurement time scale as the inverse of the driving frequency as a function of the inverse temperature corresponding to the maximum in χ'' at that frequency (symbols) and fit (drawn line) according to the Arrhenius law, with $\tau_0=(7.5\pm1.4)\times10^{-13}$ s, and $\Delta E=13.10\pm0.12$ K.

of χ' and χ'' would be equal. On further lowering of the temperature, χ'' would decrease again, but more slowly. The relaxation time as a function of temperature would not be well described by the Arrhenius law.

Although in the $[Fe_{13}]$ measurements the much smaller χ'' signal compared to χ' agrees with a spin-glass interpretation, the lack of frequency dependence of χ' does not. In addition the χ'' signal as a function of temperature is more symmetric (Lorentzian) than in a typical spin glass, and the frequency shift is also larger, viz., $\Delta T_f/T_f\Delta(\log_{10}\omega)=0.11$. Fitting the temperatures of the maxima in χ'' at the various frequencies (Fig. 9) to the Arrhenius equation, $\tau=\tau_0\exp(-\Delta E/kT)$, yields an energy barrier of $\Delta E=13.10\pm0.12$ K, and $\tau_0=(7.5\pm1.4)\times10^{-13}$ s. The prefactor τ_0 of 7.5×10^{-13} s shows that the slow relaxation is not due to strong intermolecular interactions, which would lead to much smaller values for τ_0, like in spin glasses,[20] but nevertheless it is smaller than typical values for single-molecule magnets (τ_0 is $10^{-7}-10^{-9}$ s). This combined with the fact that the Arrhenius law gives a good description of the data agrees with superparamagnetic-like behavior being the cause of the slow dynamics, as evidenced by a nonzero χ'' signal. Apparently the local disorder in $[Fe_{13}]$ as suggested by the crystal structure, causes deviations from cubic symmetry leading to finite zero-field splitting of the ground state (in agreement with the HFEPR measurements), but the random intermolecular interactions are too weak to cause spin-glass-like behavior. Since the real part of the ac susceptibility χ' is much larger than the imaginary part, it must be a minority species that shows slow relaxation of the magnetization. The majority species clearly shows no barrier toward relaxation, therefore no slow magnetization dynamics. As mentioned above, the magnitude of the χ' signal does depend on the measurement frequency. The explanation which agrees with both observations is that the majority part of the sample shows fast underbarrier tunneling of the magnetization with a wide distribution in tunneling frequencies, which would account for the lack of a temperature-dependent out-of-phase ac susceptibility signal for this part. A certain temperature-independent contribution to χ'' (as expected for a tunneling phenomenon) can be observed in Fig. 8, since χ'' does not tend to zero at the high- and low-temperature ends. The increase of χ' with decreasing frequencies reflects the fact that at increasingly lower frequencies an increasingly larger fraction of the molecules have tunneling frequencies such that they can contribute to the susceptibility. In terms of a spin Hamiltonian, the necessary transverse terms will then originate in local distortions of the symmetry as found in the x-ray studies. In short, the magnetization dynamics is very much determined by the disorder in the system, leading to a

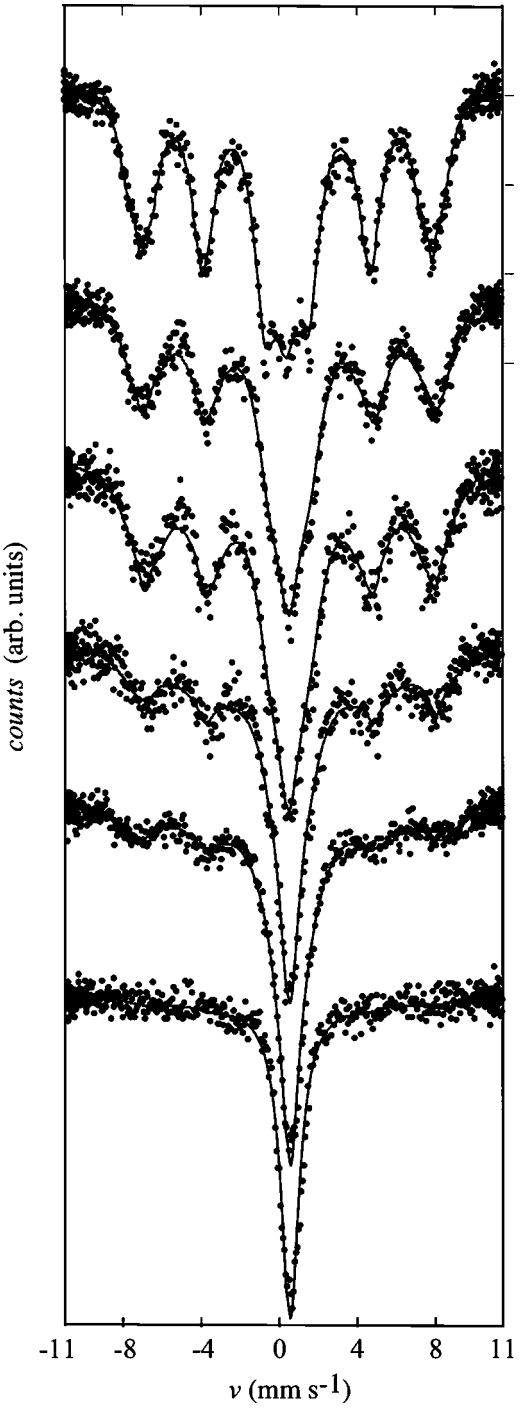

FIG. 10. Mössbauer spectra collected at (starting from the top) $T=2.55$, 3, 4, 5, 7.9, and 13 K. Solid lines represent fits obtained as described in the text.

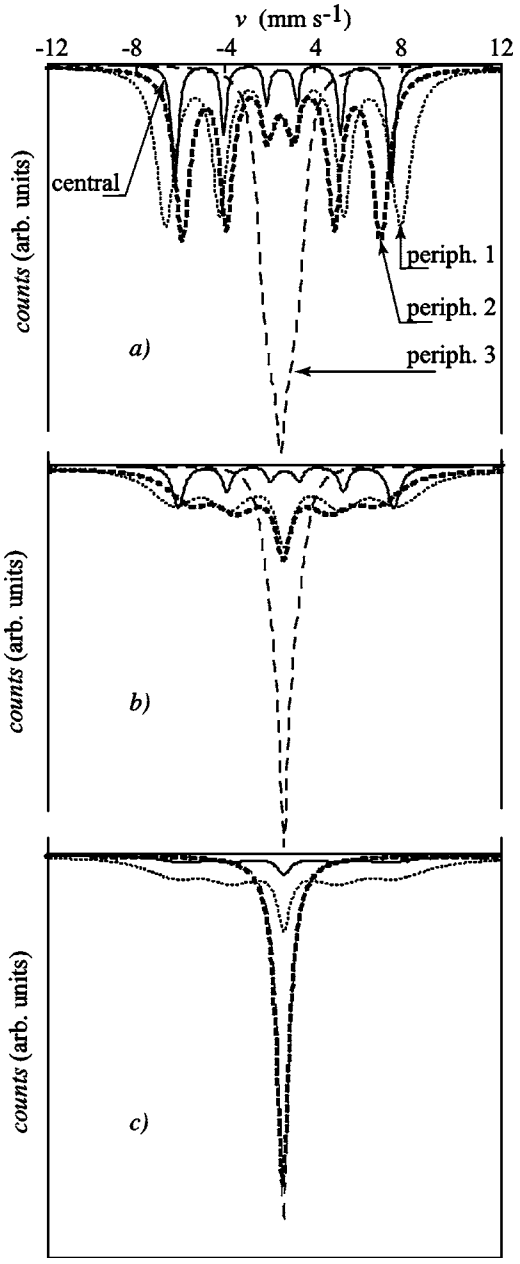

FIG. 11. Spectrum components relative to the four sites, at (a) $T=2.55$ K; (b) $T=5$ K; (c) $T=13$ K.

part of the sample relaxing over a barrier, and another part that tunnels under it.

Mössbauer spectroscopy

In order to characterize the low-temperature magnetic properties further, Mössbauer spectroscopy, which is a much shorter-timescale technique than ac susceptibility, was employed. Six spectra of 1024 channels in the ± 11 mm s^{-1} velocity range were collected between 2.55 and 13 K (Fig. 10). The 2.55 K spectrum displays a well-resolved magnetic hyperfine structure [Fig. 11(a)] that diminishes as the temperature increases and becomes almost completely absent in the 13 K spectrum [Figs. 11(b) and 11(c)]. This is indicative of a rapid increase in the spin fluctuation rate with temperature. Although the crystal structure suggests the presence of only two independent iron sites, the analysis of the 2.55 K Mössbauer spectrum showed that it is the sum of four contributions in a 1:4:4:4 ratio. This can be rationalized as follows: due to the frustration among the peripheral iron ions many equivalent topological configurations contribute to the ground state band. If the transitions between these configurations is slow on the Mössbauer timescale, in other words if the spin fluctuations are slower than the Larmor frequency of the nuclear spin around the instantaneous hyperfine field, the peripheral iron nuclei may experience different hyperfine fields, and consequently the Mössbauer spectrum would contain a contribution from each of the peripheral sites as well as that from the central iron ion. The relaxation effects on the 2.55 K spectrum are fairly small, so that the hyperfine parameters can be obtained with a good precision (Table I). The values obtained for these parameters were then used throughout the fitting processes of the other spectra. The isomer shifts of 0.40 mm s^{-1} and negligible quadrupole splittings are as expected for iron(III) ions in relatively symmetric surroundings. Interestingly, the magnetic hyperfine fields are very similar for the central and two of the peripheral sites, while a much smaller value was obtained for the third one. In the absence of an external magnetic field, the hyperfine field experienced by a high spin iron(III) nucleus (B_0^{hf}) is mainly determined by the Fermi contact term, i.e., the polarization of the *s* electrons at the nucleus by the electrons in the partially filled *d* shell, which is of the order of 55 T.[21,22] This field is modified by the exchange field in an exchange-coupled system to $B_{\mathrm{hf}}=(\langle S\rangle/S)B_0^{\mathrm{hf}}$, where $\langle S\rangle$ is the mean spin value. From these hyperfine field values, an estimate of the spin ground state value can be obtained, because the $S_z=S$ component of the cluster total spin is given by the algebraic sum of the highest values of the mean spin components s_z of the single ions. As the central-peripheral exchange interaction was calculated to be stronger than the peripheral-peripheral one, we can assume the central spin to be opposite to the resultant peripheral one and also to the two largest peripheral spins. The total cluster spin is then estimated by

$$S=\frac{2.5}{B_0^{hf}}[4(B^{(1)}+B^{(2)}-B^{(3)})-B^{(0)}], \tag{4}$$

where $B_0^{\mathrm{hf}}=50-55$ T (see above), and the superscripts (i) $(i=0,1,2,3)$ label the central site and the peripheral ones in

TABLE I. Hyperfine interaction parameters obtained from the fits of the 2.55 K Mössbauer spectrum. IS is the isomer shift, QS the quadrupolar splitting, B the hyperfine field, and I_2/I_1 the ratio of the intermediate and inner lines intensities. The numbers in parentheses denote errors in the preceding digit.

Site	IS (mm s^{-1})	QS (10^{-3} mm s^{-1})	B (T)	I_2/I_1
Central	0.41(4)	−24(3)	46.5(7)	1.8(8)
Peripheral 1	0.40(4)	−26(3)	50(1)	2.7(2)[a]
Peripheral 2	0.40(2)	−0.8(29)	43.5(3)	2.7(2)[a]
Peripheral 3	0.39(4)	37(3)	9.3(5)	2.7(2)[a]

[a]Constrained to the same value for all three peripheral sites.

TABLE II. Relaxation parameters (linewidth Γ and Blume-Tjon transition probability per unit time W) for the four sites obtained from the best fit of the spectra. Since both W and Γ contribute to the linewidths of the spectra, we have expressed also W in mm s^{-1} (see text for details). For the ^{57}Fe isotope, the equivalence of the units is; 1 mm s^{-1}=11.6 MHz. For the parameter values without an error indication, only the order of magnitude could be obtained from the fit.

	Central		Periph. 1		Periph. 2		Periph. 3	
T (K)	Γ (mm s^{-1})	W (mm s^{-1})	Γ (mm s^{-1})	W (mm s^{-1})	Γ (mm s^{-1})	W (mm s^{-1})	Γ (mm s^{-1})	W (mm s^{-1})
2.55	0.2(9)	0.1(3)	0.2(8)	0.5	0.5(9)	0.3(5)	0.8	0.3(7)
3	0.2(8)	0.3(3)	0.2(6)	0.7(8)	0.4(9)	0.8(4)	0.5	0.5(3)
4	0.2(8)	0.3(6)	0.2(9)	1.0	0.4	0.7(5)	0.5	0.5(5)
5	0.2(9)	0.3(4)	0.2	1.5	0.4	1.6(8)	0.5	0.8(6)
7.9	1	1.5	0.2(5)	1.0(8)	0.7(2)	21	1.0	1.6
13	0.8	2	0.6	2.0	0.8	93	1.0	16

the same order of Table I, resulting in a cluster total spin of $S=12-13$ in good agreement with the value $S=\frac{23}{2}$ calculated from the dc susceptibility measurements.

For the peripheral ions, the ratio of the areas of the intermediate and inner lines, is found to be 2.7 instead of 2, as would be expected for isotropic f factors,[23] which can be explained by different stiffnesses of the elastic forces in the radial and tangential directions. The same ratio is 2 for the central site, as is expected by considering the high symmetry of its surroundings.

The line shape of each subspectrum was estimated by using the simple Blume-Tjon (BT) theory.[24] In the simple BT theory, the effect of spin fluctuations on spectra is simulated by stochastic inversions of the hyperfine field, as would happen during inversion of the magnetization in a superparamagnet. Although the actual values for the linewidths (Γ) and BT transition rates (W) are only estimates (Table II), it proved to be necessary to take the BT transition rates and linewidths as free parameters for each site (Table II). This indicates that the spin dynamics cannot be simply described in terms of motion of the total spin, and that the correlations between the motions of the different sites have to be taken into account.

In the 5 K spectrum, the central-site subspectrum again displays six lines [Fig. 11(b)], while the inner lines of the peripheral-site 1 sites subspectrum and all the lines of the other peripheral subspectra are collapsed into central enlarged lines. That is, the fluctuation rate of the central spin is slower than that of the peripheral spins, as we can expect in view of the peripheral spin frustration. In the range 8–13 K, the W values increase considerably with temperature: the peripheral-2 subspectrum collapses into an enlarged central line; instead in the subspectra of the central and peripheral-1 sites, only the inner lines collapse, while the intermediate and external lines are present but in a very broadened form. This reflects the increase of the spin dynamics rate. Interestingly, using the values for the energy barrier and prefactor obtained from the Arrhenius fit of the ac susceptibility data, and the typical Mössbauer timescale of 10^{-8} s, a blocking temperature of 1.70 K is found, which is in good agreement with the observation that at 2.55 K most of the spin dynamics in the Mössbauer spectrum have been frozen.

CONCLUSIONS

Competing isotropic exchange interactions lead to a large density of close-lying spin states as shown by dc susceptibility and INS measurements. At low temperatures below 1 K, ac susceptibility measurements show that the magnetization dynamics slow down. Part of the sample shows superparamagnetic-like behavior evidenced by a frequency-dependent out-of-phase susceptibility signal, while for the other part of the sample the dynamics is limited by the tunneling frequency. By the Mössbauer spectra, the dynamics was shown to involve mainly the peripheral iron ions.

ACKNOWLEDGMENTS

We are grateful for the support from the EU RTN "Molnanomag" (Contract No. HPRN-CT-1999-00012), "Sentinel" (Contract No. HPRI-CT-2000-40022), and "Quemolna" (Contract No. MRTN-CT-2003-504880). Italian MIUR Firb and Prin projects and German DFG Schwerpunktprogramm Molekularer Magnetismus (SPP 1137), are thanked for their financial support. H.C. is grateful for a grant, Grant No. HPMF-CT-2002-02159. Professor Miguel A. Novak of the Instituto de Fisica Universidade Federal do Rio de Janeiro is kindly thanked for constructing the ac probe. We thank C. Mondelli and the technical staff of the Institute Laue Langevin for help with the INS measurements.

*Present address: 1. Physikalisches Institut, Universität Stuttgart, Pfaffenwaldring 57, D-70550 Stuttgart, Germany.
†Present address: ICMCB, CNRS-UPR9048, 87 av. du Dr. Albert Schweitzer, F-33608 Pessac, France.
‡Corresponding author.
§Present address: Leiden Institute of Chemistry, Gorlaeus Laboratories, P.O. Box 9502, NL-2300 RA Leiden, The Netherlands.
‖Present address: European Commission, Directorate General Joint Research Centre, Institute for Transuranium Elements, Postfach 2340, D-76125 Karlsruhe.

[1] J. Greedan, J. Mater. Chem. **11**, 37 (2001).
[2] A. Müller, M. Luban, C. Schröder, R. Modler, P. Kögerler, M. Axenovich, J. Schnack, P. Canfield, S. Bud'ko, and N. Harrison, ChemPhysChem **2**, 517 (2001).
[3] A. Bino, M. Ardon, D. Lee, B. Spingler, and S. J. Lippard, J. Am. Chem. Soc. **124**, 4578 (2002).
[4] F. Muller, M. A. Hopkins, N. Coron, M. Grynberg, L. C. Brunel, and G. Martinez, Rev. Sci. Instrum. **60**, 3681 (1989).
[5] A. L. Barra, L. C. Brunel, and J. B. Robert, Chem. Phys. Lett. **165**, 107 (1990).
[6] T. Steiner, Angew. Chem., Int. Ed. **41**, 48 (2001).
[7] L. Brammer, E. A. Bruton, and P. Sherwood, Cryst. Growth Des. **1**, 277 (2001).
[8] H. Weihe and H. U. Güdel, J. Am. Chem. Soc. **119**, 6539 (1997).
[9] C. Cañada-Vilalta, T. A. O'Brien, E. K. Brechin, M. Pink, E. R. Davidson, and G. Christou, Inorg. Chem. **43**, 5505 (2004).
[10] F. Le Gall, F. Fabrizi de Biani, A. Caneschi, P. Cinelli, A. Cornia, A. C. Fabretti, and D. Gatteschi, Inorg. Chim. Acta **262**, 123 (1997).
[11] M. Lahlou-Mimi and J. M. Greneche, J. Magn. Magn. Mater. **150**, 263 (1995).
[12] V. V. Volkov, Y. V. Rakitin, and V. T. Kallinikov, Koord. Khim. **7**, 1627 (1981).
[13] K. Kambe, J. Phys. Soc. Jpn. **5**, 48 (1950).
[14] E. Belorizky and P. H. Fries, J. Chim. Phys. Phys.-Chim. Biol. **90**, 1077 (1993).
[15] C. Christmas, J. B. Vincent, H.-R. Chang, J. C. Huffman, G. Christou, and D. N. Hendrickson, J. Am. Chem. Soc. **110**, 823 (1988).
[16] R. Basler, C. Boskovic, G. Chaboussant, H. U. Güdel, M. Murrie, S. T. Ochsenbein, and A. Sieber, ChemPhysChem **4**, 910 (2003).
[17] G. Chaboussant, S. T. Ochsenbein, A. Sieber, H. U. Güdel, H. Mutka, A. Muller, and B. Barbara, Europhys. Lett. **66**, 423 (2004).
[18] A. Sieber, C. Boskovic, R. Bircher, O. Waldmann, S. T. Ochsenbein, G. Chaboussant, H. U. Güdel, N. Kirchner, J. van Slageren, W. Wernsdorfer, A. Neels, H. Stoeckli-Evans, S. Janssen, F. Juranyi, and H. Mutka, Inorg. Chem. **44**, 4315 (2005).
[19] A. Cornia, R. Sessoli, L. Sorace, D. Gatteschi, A. L. Barra, and C. Daiguebonne, Phys. Rev. Lett. **89**, 257201 (2002).
[20] J. A. Mydosh, *Spin glasses: an Experimental Introduction* (Taylor & Francis, London, 1993).
[21] P. Gütlich and J. Ensling, in *Inorganic Electronic Structure and Spectroscopy, Volume I: Methodology*, edited by E. I. Solomon and A. B. P. Lever (John Wiley & Sons, New York, 1999).
[22] M. F. Thomas and C. E. Johnson, in *Mössbauer Spectroscopy*, edited by D. P. E. Dickinson and F. J. Berry (Cambridge University Press, Cambridge, 1986).
[23] C. Janot, *L'effet Mössbauer et ses Applications* (Masson et C., Paris, 1972).
[24] M. Blume and J. A. Tjon, Phys. Rev. **165**, 446 (1968).